metals

MDPI

Article

Influence of the Quenching and Partitioning Process on the Transformation Kinetics and Hardness in a Lean Medium Manganese TRIP Steel

Simone Kaar [1,*], Reinhold Schneider [1], Daniel Krizan [2], Coline Béal [3] and Christof Sommitsch [3]

[1] Research and Development, University of Applied Sciences Upper Austria, Wels 4600, Austria; reinhold.schneider@fh-wels.at
[2] Research and Development Department, Business Unit Coil. Voestalpine Steel Division GmbH, Linz 4020, Austria; daniel.krizan@voestalpine.com
[3] Institute of Materials Science, Joining and Forming, Graz University of Technology, Graz 8010, Austria; coline.beal@tugraz.at (C.B.); christof.sommitsch@tugraz.at (C.S.)
* Correspondence: simone.kaar@fh-wels.at; Tel.: +43-50304-15-6250

Received: 27 February 2019; Accepted: 16 March 2019; Published: 19 March 2019

Abstract: The quenching and partitioning (Q&P) process of lean medium Mn steels is a novel approach for producing ultra-high strength and good formable steels. First, the steel is fully austenitized, followed by quenching to a specific quenching temperature (T_Q) in order to adjust an appropriate amount of initial martensite ($\alpha'_{initial}$). Subsequently, the steel is reheated to a partitioning temperature (T_P) in order to ensure C-partitioning from $\alpha'_{initial}$ to remaining austenite (γ_{remain}) and thus retained austenite (RA) stabilization. After isothermal holding, the steel is quenched to room temperature (RT), in order to achieve a martensitic-austenitic microstructure, where the meta-stable RA undergoes the strain-induced martensitic transformation by the so-called transformation induced plasticity (TRIP) effect. This paper systematically investigates the influence of the Q&P process on the isothermal bainitic transformation (IBT) kinetics in a 0.2C-4.5Mn-1.3Al lean medium Mn steel by means of dilatometry. Therefore, the Q&P annealing approach was precisely compared to the TRIP-aided bainitic ferrite (TBF) process, where the samples were directly quenched to the temperature of the IBT after full austenitization. The results indicated an accelerated IBT for the Q&P samples, caused by the formation of $\alpha'_{initial}$ during quenching below the martensite start (M_S) temperature. Furthermore, a significant influence of the annealing parameters, such as T_Q and T_P, was observed with regard to the transformation behavior. For further characterization, light optical microscopy (LOM) and scanning electron microscopy (SEM) were applied, showing a microstructure consisting of a martensitic-bainitic matrix with finely distributed RA islands. Saturation magnetization method (SMM) was used to determine the amount of RA, which was primarily depending on T_Q. Furthermore, the hardness according to Vickers revealed a remarkable impact of the annealing parameters, such as T_Q and T_P, on the predicted mechanical properties.

Keywords: Q&P; TRIP; lean medium Mn steel; transformation kinetics

1. Introduction

Both environmental and safety regulations force the automotive industry to the application of new steel grades [1,2]. In order to meet the challenging requirements concerning crashworthiness, formability, and reduction of CO_2 emissions, "Advanced High Strength Steels" (AHSS) are currently under development [3–5]. By the increase of the material strength without a deterioration of ductility, the sheet thickness can be downgauged, resulting in a significant weight reduction of the body structures [1,6]. Furthermore, the combination of both high strength and ductility is of vital importance

in order to manufacture complex automotive parts. Therefore, a high research effort has been put into the further development of AHSS.

The 1st generation AHSS, being already in industrial application, is represented by Dual Phase (DP), TRIP, and Complex Phase (CP) steels [6]. These steels mainly have a multiphase structure, resulting in tensile strengths up to 1200 MPa and total elongations up to 40% [7–9]. Typically, they are characterized by R_mxA_{80} up to 20,000 MPa% [6]. The 2nd generation AHSS includes Twinning Induced Plasticity (TWIP), Nano-TWIP, Duplex, and Triplex steels, which are characterized by highly promising mechanical properties, especially an excellent combination of strength and ductility with R_mxA_{80} between 40,000 and 60,000 MPa% [10]. However, due to the high alloying costs and challenging processing they are hardly used in industrial applications [11].

Currently, recent research activities focus on the development of steels belonging to the 3rd generation AHSS, including the concepts of Q&P and medium Mn steels, to fill the property gap between the 1st and 2nd generation AHSS [9,12–14].

The Q&P process has been proposed as a promising approach for steel grades having the microstructure consisting of a carbon-depleted martensitic matrix and retained austenitic islands [15]. In this process, the steel is fully austenitized followed by quenching to a specific temperature below the M_S temperature, where the optimal amount of RA can be adjusted. Subsequent reheating and holding in the over-ageing region triggers the α' tempering, whereby the cementite formation during this stage will be significantly postponed by the Si and/or Al additions. Therefore, C can partition to remaining γ resulting in its appropriate stabilization upon final cooling to room temperature (RT) [16,17].

The medium Mn steels typically contain between 3 and 10 wt.% Mn and their microstructure consists of an ultrafine-grained ferritic matrix (with a typical grain size below 1 µm) and approximately 30 vol.% of RA. These steel grades are characterized by an excellent combination of tensile strength and total elongation achieving the product of R_mxA_{80} exceeding 30,000 MPa% [12,14,18].

In the present case, the concept of lean medium Mn Q&P steels combines both the approach of medium Mn steels and the Q&P process, leading to a microstructure consisting of a tempered martensitic matrix with an increased amount of RA islands. The RA can be stabilized by the combination of the C and Mn enrichment, ensuring an optimum strain-induced γ to α' transformation (TRIP-effect). Moreover, the presence of the hard C-depleted martensitic matrix ensures the superior performance of these steels in the forming operations such as sheet cutting, bending and hole expansion, since the ability to resist high local strains is linked to the hardness gradients in the microstructure [19].

In order to predict the amount of RA depending on T_Q, the constrained carbon equilibrium (CCE) model proposed by Speer et al. [20] can be applied. This simplified model allows the calculation of the C-content in γ and therefore the prediction of the amount of RA under three main conditions: (1) All of the C partitions to γ and the partitioning kinetics are ignored, meaning the partitioning is already complete; (2) no phase boundary movement during the partitioning process; and (3) no competing reactions like carbide or α_B formation take place during the Q&P process [20].

However, the decomposition from γ to α_B during the C-partitioning step has been observed in some instances [21–23]. Clarke et al. [24] showed that the formation of carbide-free bainite (α_B) during the partitioning process led to a reduced RA fraction in the Q&P samples compared to the amounts predicted by the CCE-model. However, in some cases, the formation of α_B can contribute to the stabilization of γ by its C-enrichment.

Therefore, in the present paper, the transformation behavior of a 0.2-4.5Mn-1.3Al steel was studied for both Q&P and TBF processes in order to evaluate the influence of the presence of $\alpha'_{initial}$ on IBT. Several annealing parameters were varied (T_Q, T_P), in order to examine their influence on the transformation kinetics and thus the volume fraction of the individual constituents, i.e., α', α_B, and RA, in the final microstructure.

2. Materials and Methods

Table 1 shows the chemical composition of the investigated steel grade in wt.%. The steel was melted in a medium frequency induction furnace and cast under laboratory conditions in an ingot of 80 kg. First the material was hot rolled to a thickness of 4 mm, followed by tempering in a batch-annealing-like furnace at a temperature of 550 °C for 16 h. Finally, the material was cold rolled to a thickness of 1 mm.

Table 1. Chemical composition of the investigated steel Fe-C-Mn-Al in wt.%.

C	Mn	Al	Si
0.20	4.49	1.30	0.04

The transformation behavior and the influence of the different annealing parameters were investigated by means of dilatometry using a Bähr 805 A/D dilatometer. Therefore, specimens with dimensions of 10 × 4 × 1 mm^3 were produced by wire-electrical discharge machining. Figure 1 shows the applied time-temperature schedules for the Q&P (a) and the TBF (b) heat-treatments, adapted to suit an industrially feasible continuous annealing line. All samples were fully austenitized at a T_{an} of 900 °C for 120 s (t_{an}) with a heating rate HR_1 of 10 K/s. For the Q&P process, the austenitization was followed by quenching to various T_Q in the range of 130 °C–330 °C with a 20 °C step using a cooling rate CR_1 of 50 K/s. The T_Q was held for 10s and subsequently the samples were reheated with 20 K/s (HR_2) to a certain T_P, which was varied between 350, 400, and 450 °C and held for 600 s (t_p), respectively. In contrast, the TBF samples were directly cooled to a T_B of 350, 400, or 450 °C and held for 600 s (t_B). Finally, both Q&P and TBF samples were cooled to RT with a cooling rate CR_2 of 50 K/s.

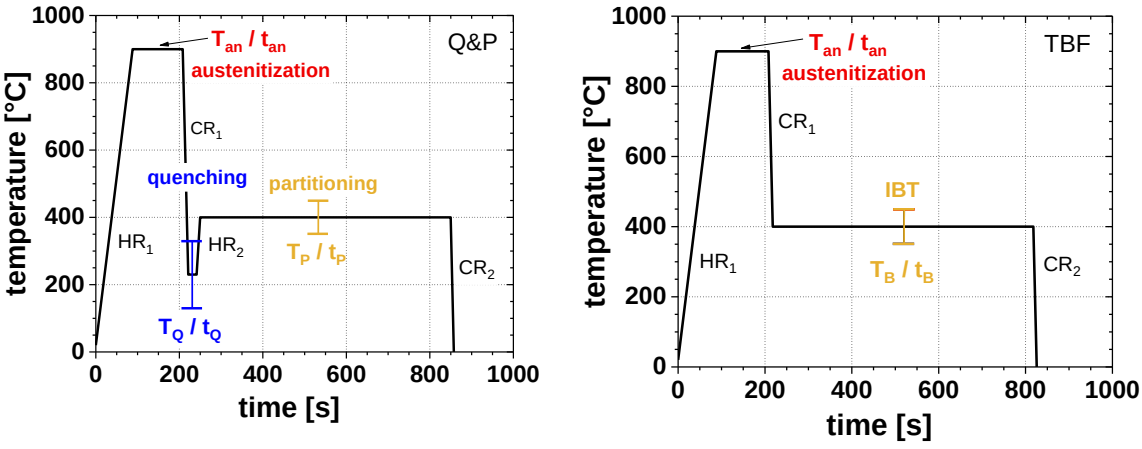

Figure 1. Time-temperature regimes used for (**a**) the quenching and partitioning (Q&P) and (**b**) the transformation induced plasticity (TRIP) aided bainitic ferrite (TBF) heat-treatments.

The microstructure was characterized by means of light optical microscopy (LOM) using LePera etching [25]. Furthermore, the samples were electrochemically polished for the SEM investigations. Vickers hardness testing (HV1) was performed on polished samples using an Emco Test DuraScan 20 device. The volume fraction of RA was determined by the use of SMM [26]. Furthermore, the RA content depending on the T_Q was calculated using the CCE-model proposed by Speer et al. [20]. Therefore, first the volume fraction of α' formed during quenching to T_Q was determined by the Koistinen-Marburger (KM) equation, which can be used to predict the γ to α' transformation rate and is given by [27]:

$$f_M = 1 - e^{-0.011(M_S - T_Q)}$$

Here, f_M is the fraction of α' transformed during quenching from the γ-region to the T_Q. M_S is the martensite start temperature, which was calculated according to Mahieu et al. [28]:

$$M_S = 539 - 423\text{C} - 30.4\text{Mn} - 7.5\text{Si} + 30\text{Al}$$

Figure 2a displays the phase fractions of α' and γ determined using the CCE-model and Figure 2b represents the related Q&P heat-treatment. Both, KM- and M_S-formula are applied twice in the CCE-model. First, the M_S temperature of the initial γ is calculated, followed by the determination of the α' fraction formed during quenching to a certain T_Q using the KM equation (blue line). The orange curve represents the remaining initial γ after quenching. Subsequently, the M_S temperature of the C-enriched γ after the partitioning step is calculated assuming full C-partitioning from α'. Given that, using the KM equation once again, the amount of α' formed upon final cooling to RT is calculated (red line). The resulting RA fraction as a function of the T_Q is indicated in green. It is evident that the largest fraction of γ can be retained at that T_Q where no fresh α' is formed upon final cooling. However, it must be taken into account that this applied CCE-model does not consider a phase transformation from γ to α_B during isothermal holding at T_P. Since this contribution focusses on the investigation of the bainitic transformation kinetics during Q&P processing, it can be expected that the amount of retained austenite stabilized to RT will be smaller, compared to the calculated one.

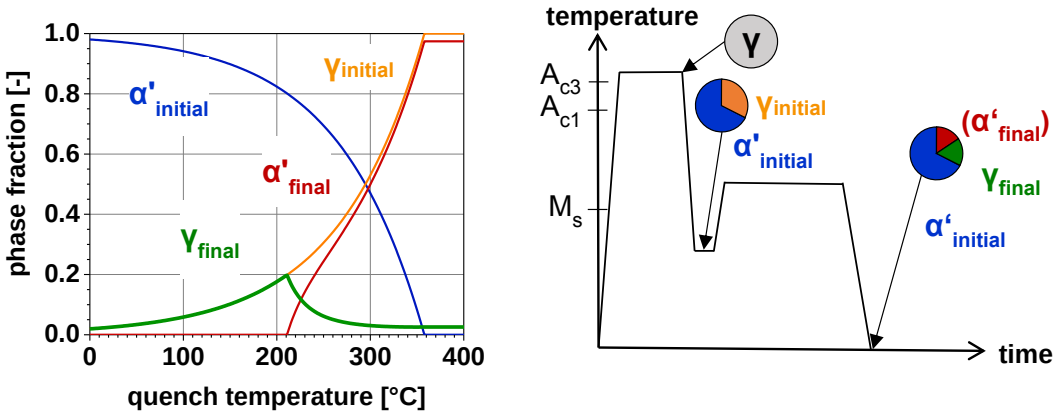

(**a**) (**b**)

Figure 2. (**a**) Calculated phase fractions of martensite (α') and austenite (γ) depending on the T_Q and (**b**) the related Q&P heat-treatment with the schematic microstructural evolution; the phase fractions are indicated for the initial quench to T_Q and for the final quench to room temperature (RT).

3. Results

3.1. Transformation Behavior

The annealing parameters, especially T_Q and T_P, remarkably influenced the transformation behavior of the investigated steel. Figure 3 shows the influence of the T_P-variation in a range of 350–450 °C on the dilatometric curves using the Q&P heat-treatment with a T_Q of 310 °C (Figure 3a) compared to the TBF cycles (Figure 3b). After full austenitization at 900 °C, the dilatometric samples were cooled to T_Q or T_B, depending on the applied heat-treatment. In the case of the Q&P regime, α'_{initial} was formed during quenching to T_Q, since the M_S temperature was approximately 325 °C (Figure 3a). Although the CCE-model, describing the microstructural development during Q&P processing, assumes full C-partitioning from γ to α' without the occurrence of any phase transformations during isothermal holding at T_P, in the present case after reheating to T_P, γ partially transformed to α_B during isothermal holding, accompanied by a linear expansion visible in the dilatometric curves. Further, it is obvious that the amount of α_B described by the volume expansion during isothermal holding decreased with increasing T_P. As a result, T_P directly influenced the

formation of α'_{final} during cooling to RT. For the Q&P sample heat-treated at a T_P of 350 °C, no α'_{final} was formed, whereas at an increased T_P of 400 and 450 °C, a $\gamma \rightarrow \alpha'_{final}$ transformation was observed by a deviation from the linearity of the dilatometric curves during final cooling. In contrast, for the TBF samples, the largest amount of α_B was formed at a T_B of 400 °C, whereas its smallest amount was contemplated at 450 °C. The correlation between the amount of α_B and α'_{final} was proven for the TBF regime as well. Thus, the largest amount of α'_{final} was transformed at a T_B of 450 °C, whereas the lowest α' formation was obtained at 400 °C.

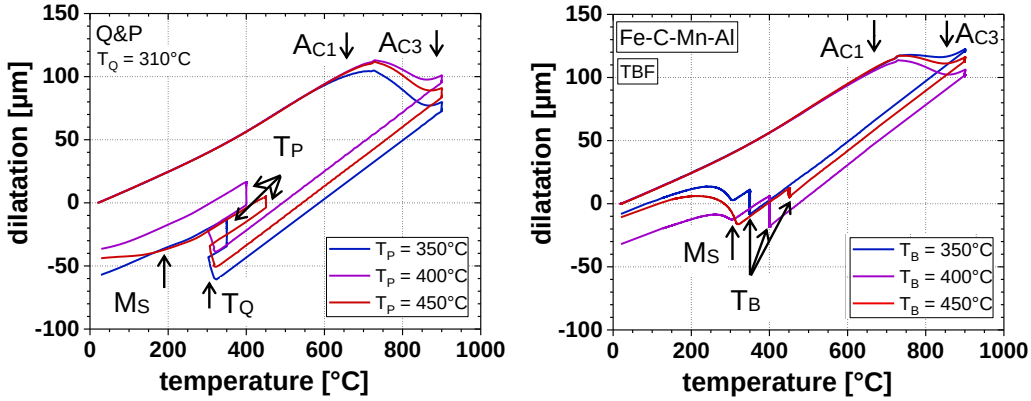

(**a**) (**b**)

Figure 3. Dilatometric curves at different T_P (T_B) of (**a**) Q&P heat-treatment (T_Q = 310 °C) and (**b**) TBF heat-treatment.

The influence of T_P or T_B on the α_B formation during isothermal holding for the Q&P (T_Q = 310 °C) and TBF process is displayed in detail in Figure 4. For both the Q&P and TBF regimes, an increasing T_P and T_B led to accelerated IBT kinetics. However, with an increase of T_P and T_B, the α_B formation saturated already after shorter times. In the case of the Q&P samples, this behavior led to the largest amount of α_B at a T_P of 350 °C, whereas with increasing T_P, lower α_B fractions were formed during isothermal holding. On the one hand, the IBT in the TBF regime was remarkably slower compared to that of the Q&P process. On the other hand, the IBT did not saturate at a T_B of 350 °C and 400 °C, even after a t_B of 600 s.

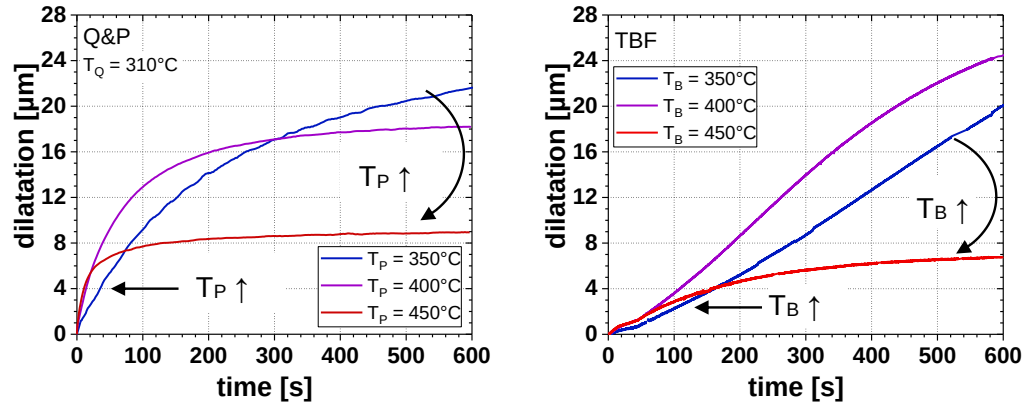

(**a**) (**b**)

Figure 4. Dilatation due to α_B formation as a function of isothermal holding time at different T_P (T_B) for (**a**) Q&P steel (T_Q = 310 °C) and (**b**) TBF steel.

Furthermore, an influence of T_Q on the transformation behavior could be determined by means of dilatometry (Figure 5). With increasing T_Q, the amount of $\alpha'_{initial}$ decreased, whereas the amount of

α_B formed during isothermal holding at T_P increased. However, too high T_Q led to the formation of α'_{final} during final cooling to RT, especially at a T_P of 450 °C.

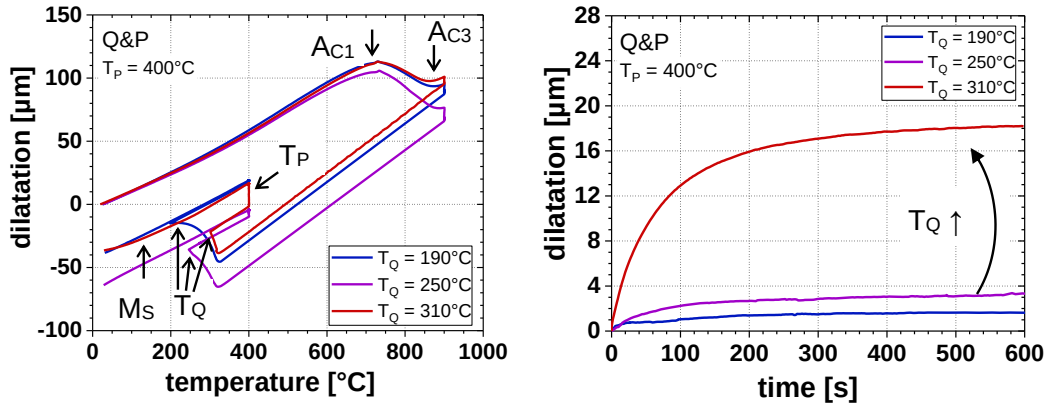

Figure 5. (**a**) Dilatometric curves at different T_Q (T_P = 400 °C) and (**b**) dilatation due to α_B formation as a function of isothermal holding time at different T_Q (T_P = 400 °C).

3.2. Microstructure

The annealing parameters, especially T_Q, significantly influenced the microstructural constitution of the investigated samples. Figure 6a–c shows the LOM images of the Q&P samples, quenched to a temperature of 190, 250, and 310 °C, respectively. In comparison, the microstructure of the sample annealed in the TBF regime is shown in Figure 6d. All four conditions were heat-treated at a T_P (T_B) of 400 °C. For the Q&P steels, the matrix consisted of a mixture of $\alpha'_{initial}$ and α_B, which appeared as bluish and brownish areas in the micrographs. Furthermore, RA and/or α'_{final} islands (white and brownish areas) could be observed as finely distributed in the matrix. At the lowest T_Q of 190 °C, the secondary phase only consisted of RA, whereas the increase of T_Q led to the pronounced formation of α'_{final}. The microstructure, especially at a T_Q of 250 and 310 °C exhibited a banded structure, resulting from the segregation of alloying elements such as Mn during casting and subsequent solidification. In contrast, the microstructure of the TBF samples consisted of a ferritic-bainitc matrix with small amounts of finely distributed RA islands, surrounded by large fractions of α'_{final}.

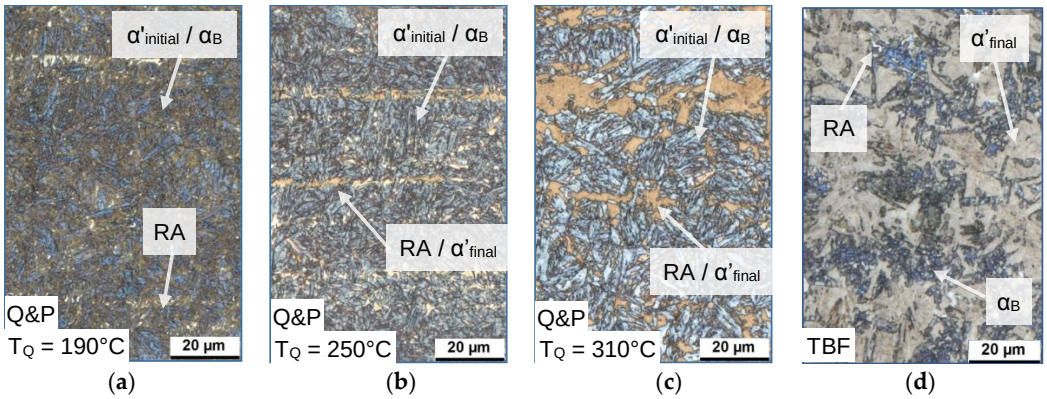

Figure 6. Light optical microscopy (LOM) images of the (**a**–**c**) Q&P samples (T_Q = 190, 250, and 310 °C) and (**d**) TBF sample at a T_P (T_B) of 400 °C (magnification 1000×).

For higher resolution investigations, the microstructure was further characterized by SEM. The SEM images of the Q&P samples quenched to a T_Q of 190, 250, and 310 °C are displayed in Figure 7a–c, whereas in Figure 7d the microstructure after the TBF heat-treatment is shown for comparison. In the case of the Q&P samples, the microstructure contained cementite precipitates with

an obvious triaxial alignment, which means that the precipitations are arranged in an angle of 120°. This indicates the presence of tempered $\alpha'_{initial}$. Furthermore, the fraction of α_B in the matrix rose along with the amount of α'_{final} with increasing T_Q. In comparison, the microstructure of the TBF steel consisted of a α_B-matrix with large amounts of α'_{final} and low fractions of RA.

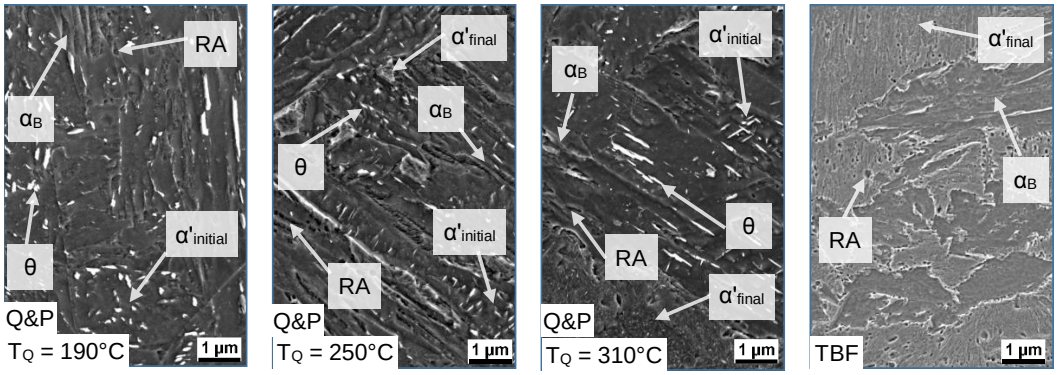

Figure 7. SEM images of the (**a**–**c**) Q&P samples (T_Q = 190, 250, and 310 °C) and (**d**) TBF sample at a T_P (T_B) of 400 °C (magnification 5000×).

Figure 8 depicts the amount of RA, determined by SMM, for the TBF samples (dotted lines) and the Q&P samples at a T_P of 350, 400, and 450 °C, respectively. In addition, the RA fraction calculated according to the CCE-model proposed by Speer et al. [20] is presented in the diagram. The CCE-model proposed a RA maximum (RA_{max}) of 19.7 vol.% at a T_Q of 210 °C. In accordance with the model calculations, the experiments also confirmed the shape of the RA evolution as a function of T_Q. At lower T_Q the formation of high amounts of $\alpha'_{initial}$ led to lower RA fractions. By a further increase of the T_Q, the RA_{max} was achieved followed by a decrease of the RA. This was due to its lower stabilization and therefore the formation of α'_{final} upon cooling to RT. Furthermore, the experiments showed an influence of T_P on the amount of RA: with increasing T_P, RA_{max} rose from 14.8 to 19.0 vol.%. In this context, at the T_P of 450 °C, the amount of RA correlated well with the model calculations. On the contrary, at the T_P of 350 °C and 400 °C, a lower amount of RA was achieved compared to the model predictions. Moreover, the T_Q at which the RA_{max} occurred, was shifted to higher temperatures by up to 80 °C compared to the CCE-model. It is evident that the RA contents of the TBF samples were lower compared to the Q&P samples: 7.1 vol.% RA at a T_B of 350 °C, 9.7 vol.% RA at T_B = 400 °C, and 3.6 vol.% RA at T_B = 450 °C.

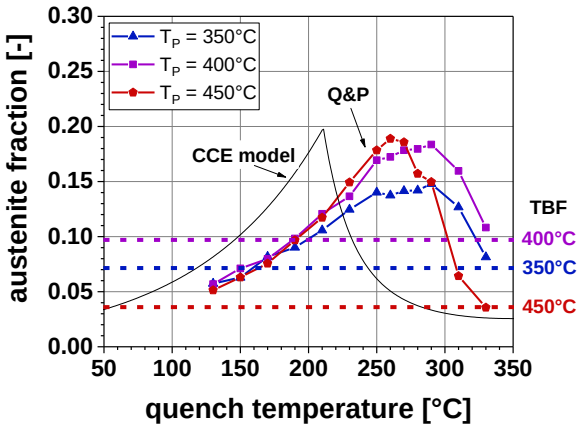

Figure 8. Retained austenite (RA) content as a function of T_Q for a T_P (T_B) of 350, 400, and 450 °C.

Figure 9 represents microstructure charts, where the phase fractions are plotted as a function of T_Q for different T_P. In addition, the bar charts, situated close to the right rim of each diagram, depict the microstructural constitution for the TBF steel. In case of the Q&P samples, the decrease of T_Q led to a considerable increase of $\alpha'_{initial}$. As a consequence, a lower amount of α_B was formed during IBT, regardless of T_P. However, particularly at higher T_Q, a vivid influence of T_P is obvious: the increase of T_P led to a decreasing fraction of α_B, resulting in the formation of α'_{final} upon cooling to RT. Therefore, the RA content steadily rose with increasing T_Q until the onset of the formation of α'_{final} occured. For the TBF samples, it is evident that the largest amount of α_B was formed at a T_B of 400 °C as already shown by dilatometry (Figure 4b). Due to the lowest α_B fraction at a T_B of 450 °C, the largest amount of γ transformed to α'_{final} during final cooling, resulting in the lowest amount of RA, followed by the samples heat-treated at a T_B of 350 °C and 400 °C.

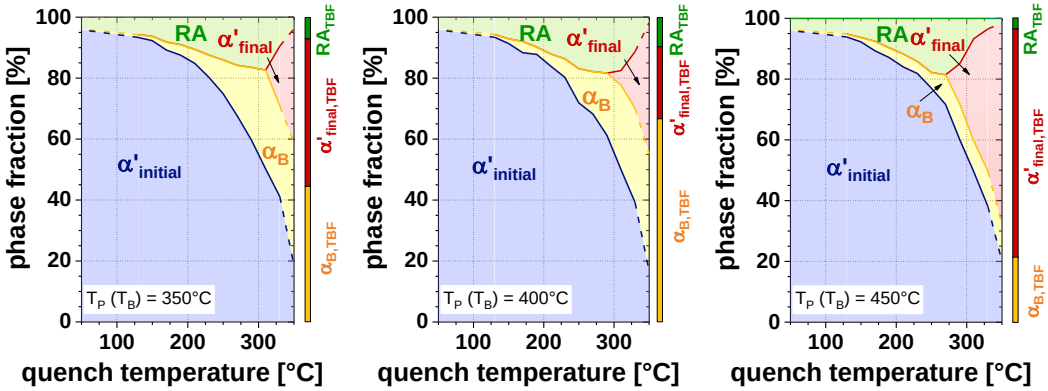

Figure 9. Phase fraction as a function of T_Q for a T_P (T_B) of (**a**) 350 °C, (**b**) 400 °C, and (**c**) 450 °C.

3.3. Hardness

The results of the hardness measurements according to Vickers are plotted as a function of T_Q in Figure 10. When the T_Q was in the range of 130 to 250 °C, both increasing T_Q and T_P led to a slightly decreasing hardness. However, at T_Q exceeding 250 °C, the hardness rose with T_Q, especially at a T_P of 450 °C. For this reason, in case of the Q&P samples, the hardness was between approximately 350 and 460 HV1. In contrast, for the TBF samples the lowest hardness of 445 HV1 was measured at a T_B of 400 °C, whereas at a T_B of 350 and 450 °C the hardness reached approximately 470 and 475 HV1, respectively.

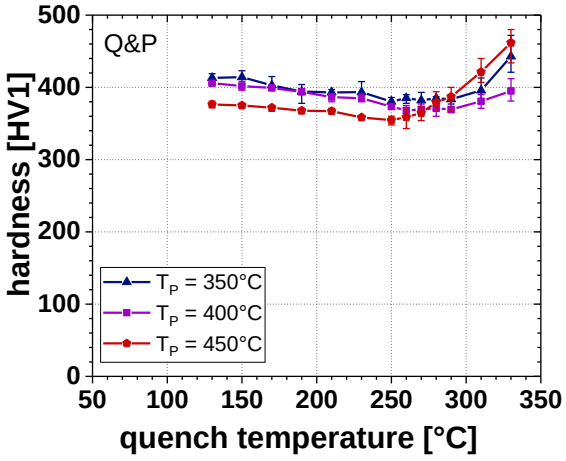

Figure 10. Vickers hardness as a function of T_Q for a T_P of 350, 400, and 450 °C.

4. Discussion

The time-temperature-transformation (TTT) diagrams for isothermal holding at different T_P (T_B) depict the comparison between the Q&P heat-treatment (Figure 11a–c) at different T_Q (190, 250, and 310 °C) and the TBF processing route (Figure 11d). It is obvious that the application of the Q&P process resulted in an evident acceleration of the α_B formation. This is in agreement with Wang et al. [29], since the presence of $\alpha'_{initial}$ pronouncedly accelerated the IBT due to the enhanced nucleation rate by the presence of geometrically necessary dislocations. At higher T_Q, the amount of α_B significantly increased, in particular at the lower T_P of 350 and 400 °C. According to Smanio and Sourmail [30], this relation can be explained by the fact that at higher T_Q lower amounts of $\alpha'_{initial}$ were formed, which was also confirmed by the LOM and SEM investigations (Figures 6 and 7). As a result, a larger amount of γ was present in the microstructure at the onset of isothermal holding, from which a larger amount of α_B could be formed, compared to lower T_Q. For this reason, the largest α_B formation was observed in the TBF samples, where especially a lower T_B of 350 °C led to increased α_B fractions up to 80 vol.% after the investigated holding time. Furthermore, a general impact of the T_P (T_B) on the transformation kinetics was found: especially at a T_P (T_B) of 400 and 450 °C the transformation kinetics was evidently accelerated due to the faster C diffusion into the remaining γ. In general, the increase of T_P and T_B led to lower fractions of α_B, which is in analogy with the T_0-concept [31]. Thereby, the difference between the Gibbs free energies of γ and α decreases with an increase of temperature. As a consequence, the driving force for α_B formation diminishes with temperature.

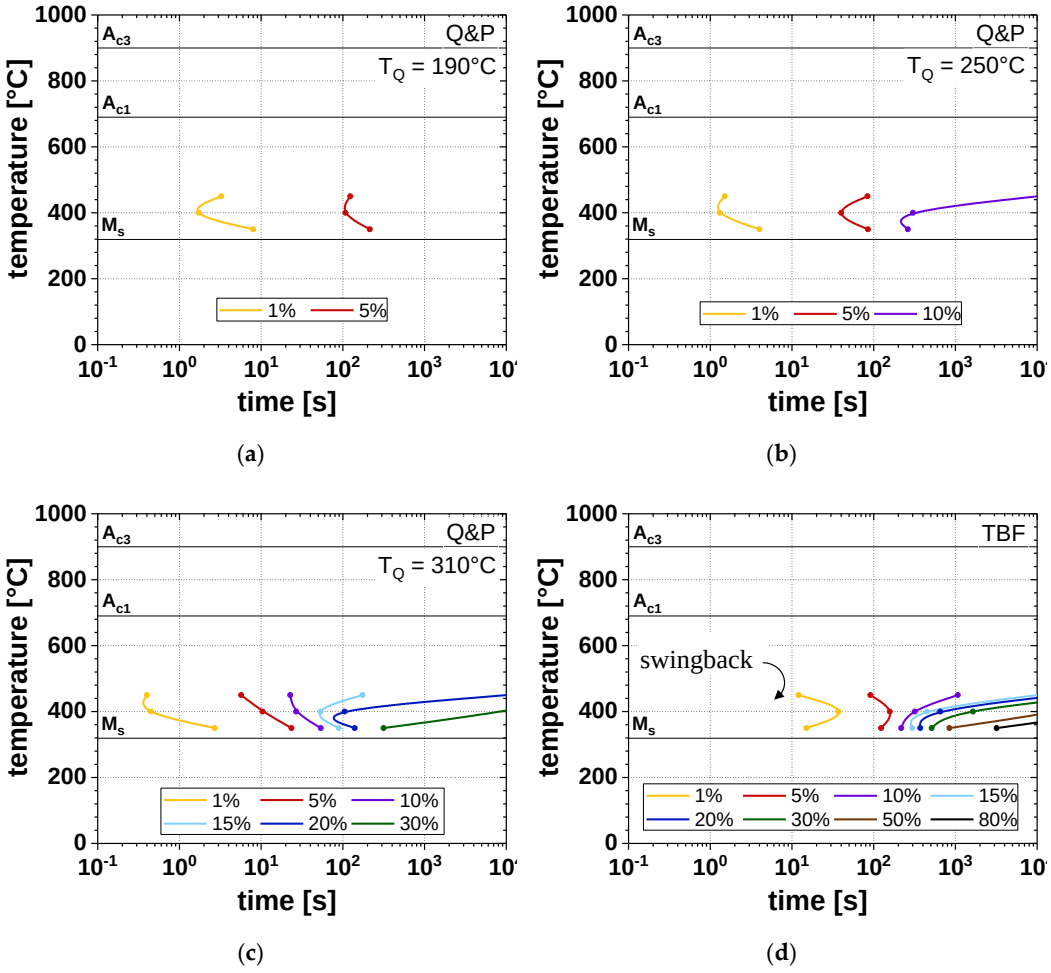

Figure 11. Time-temperature-transformation (TTT) diagrams for (**a**–**c**) Q&P steels (T_Q = 190, 250, and 310 °C) and (**d**) TBF steels.

In the case of the TBF samples, the swing back phenomenon could be contemplated, which is in accordance with Oka and Okamoto [32]. This effect describes the accelerated formation of α_B due to the formation of thin-plate isothermal α' in a temperature range just above M_S. Therefore, at a T_B of 350 °C, the onset of the α_B formation was observed at shorter times compared to a T_B of 400 °C.

Considering the RA investigations, a significant difference between the calculated CCE-model and experimental data was determined. This was particularly apparent for the amount of RA and optimal T_Q. In analogy to the present results, these observations have already been reported in the literature [24,33,34]. The CCE-model assumes full C-partitioning from $\alpha'_{initial}$ into the remaining γ. However, in the present study the microstructural investigations have shown the presence of cementite precipitates in the tempered $\alpha'_{initial}$ (Figure 7), which contradicts this assumption. The insufficient C-partitioning led to a reduced C-content in the remaining γ, resulting in a lower amount of RA due to the formation of α'_{final}, caused by the lower chemical RA stability. In particular, for the T_P of 350 °C, the RA_{max} was remarkably lower than the predicted one. According to Clarke et al. [24], the α_B formation, which predominantly occurred at a T_P of 350 °C in the present study, led to a pronounced decrease in RA as the aftermath of the reduction of untransformed γ during isothermal holding.

Furthermore, the microstructural changes were reflected in hardness according to Vickers, as well (Figures 9 and 10). With increasing RA, content hardness steadily decreased, resulting in the lowest hardness for those samples containing the largest amount of RA. Since with increasing T_P the volume fraction of RA stabilized to RT rose, the lowest hardness values could be obtained at T_P = 450 °C. However, the increased RA content at higher T_P led to the lower chemical RA stability, and thus to an intensified formation of α'_{final}. Therefore, especially at T_P = 450 °C, hardness drastically increased at T_Q, exceeding that temperature where the maximum RA content was measured. This is in agreement with [35], where a comparable correlation between the microstructural constituents (i.e., RA and α'_{final}) and resulting hardness was found for lean medium Mn steels.

The evident shift of the RA_{max} to higher T_Q than predicted could be explained by the fact that γ is stabilized by both chemical and mechanical factors, whereas the CCE-model only takes the chemical stabilization into account [36]. Furthermore, the CCE-model includes two empirical formulas, describing the α' kinetics and the M_S temperature. According to Kim et al. [37], slight differences in the chemical composition or the initial microstructure could therefore lead to deviations from the model, as well. In the present contribution, small deviations between the M_S temperature calculated according to Mahieu et al. (M_S = 350 °C) and the M_S temperature determined by means of dilatometry (M_S = 325 °C, Figure 5a) could be observed, as well. Therefore, an adjustment of the applied M_S-formula with an improved validity for increased Mn and C contents is intended for future investigations. Nevertheless, the CCE-model proposed by Speer et al. [20] is a vital tool for the first estimation of applicable annealing parameters in the case of Q&P steels.

5. Conclusions

The results of the present contribution give conclusive evidence that the Q&P process significantly influences the transformation behavior of the investigated lean medium Mn steel. Both T_Q and T_P must be carefully adjusted, since they have a substantial impact on the microstructural evolution during steel processing.

The main findings of the present study are as follows:

- The Q&P heat-treatment accelerated the transformation kinetics during isothermal holding in the partitioning step due to the presence of $\alpha'_{initial}$, which acted as nucleation sites for the α_B formation.
- For both Q&P and TBF grades, the increase of T_P (T_B) resulted in lower amounts of α_B, although the transformation kinetics was accelerated.
- With increasing T_Q, smaller amounts of $\alpha'_{initial}$ and larger amounts of α_B were formed, leading to an increased RA content. At too high T_Q, α'_{final} was formed, resulting in a sharp decrease in

RA. Therefore, the microstructure of the Q&P samples consisted of tempered $\alpha'_{initial}$, RA, and at higher T_Q partially of α_B and α'_{final}.

- The microstructure of the TBF samples with the present lean medium Mn composition consisted of a ferritic-bainitic matrix with large amounts of α'_{final} and low fractions of RA.
- The comparison of the CCE-model and the experimental data showed a significant deviation of the maximum RA content, in particular at lower T_P. Furthermore, the optimum T_Q was shifted to higher temperatures compared to the CCE-model predictions.

Author Contributions: Conceptualization, R.S., D.K., and C.S.; methodology, S.K.; software, S.K.; validation, D.K. and R.S.; formal analysis, S.K.; investigation, S.K.; resources, D.K., R.S., and S.K.; data curation, S.K., R.S., D.K., C.B., and C.S.; writing—original draft preparation, S.K.; writing—review and editing, R.S., D.K., C.B., and C.S.; visualization, S.K.; supervision, R.S., D.K., C.B., and C.S.; project administration, D.K., R.S., and C.S.; funding acquisition, D.K.

Funding: This research was funded by the Austrian Research Promotion Agency (FFG), grant number 860188, "Upscaling of medium Mn-TRIP steels".

Conflicts of Interest: The authors declare no conflict of interest. The funders had no role in the design of the study; in the collection, analyses, or interpretation of data; in the writing of the manuscript, or in the decision to publish the results.

References

1. Kwon, O.; Lee, K.; Kim, G.; Chin, K. New trends in advanced high strength steel—Developments for automotive application. *Mater. Sci. Forum* **2010**, *638–642*, 136–141. [CrossRef]
2. Spenger, F.; Hebesberger, T.; Pichler, A.; Krempaszky, C.; Werner, E.; Doppler, C. AHSS steel grades: Strain hardening and damage as material design criteria. In Proceedings of the International Conference on New Developments in Advanced High Strength Sheet Steels, Orlando, FL, USA, 15–18 June 2008; pp. 39–49.
3. Jacques, P.J.; Petein, A.; Harlet, P. Improvement of mechanical properties through concurrent deformation and transformation: New steels for the 21st century. In Proceedings of the International Conference on TRIP-aided High Strength Ferrous Alloys, Aachen, Germany, 19–21 June 2002; pp. 281–285.
4. Hashimoto, K.; Yamasaki, M.; Fujimura, K.; Matsui, T.; Izumiya, K. Global CO_2 recycling—Novel materials and prospect for prevention of global warming and abundant energy supply. *Mater. Sci. Eng. A* **1999**, *267*, 200–206. [CrossRef]
5. Zaefferer, S.; Ohlert, J.; Bleck, W. A study of microstructure, transformation mechanisms and correlation between microstructure and mechanical properties of a low alloyed TRIP steel. *Acta Mater.* **2004**, *52*, 2765–2778. [CrossRef]
6. Matlock, D.; Speer, J.; De Moor, E.; Gibbs, P. Recent developments in advanced high strength steels for automotive applications: An overview. *JESTECH* **2012**, *15*, 1–12.
7. De Cooman, B.C. Structure-properties relationship in TRIP steels containing carbide-free bainite. *Solid State Mater. Sci.* **2004**, *8*, 285–303. [CrossRef]
8. Hairer, F.; Krempaszky, C.; Tsipouridis, P.; Werner, E.; Satzinger, K.; Hebesberger, T.; Pichler, A. Effects of heat treatment on microstructure and mechanical properties of bainitic single- and complex-phase steel. *Proc MS&T* **2009**, *2009*, 1391–1401.
9. Samek, L.; Krizan, D. Steel—Material of choice for automotive lightweight applications. In Proceedings of the International Conference on Metals, Brno, Czech Republic, 23–25 May 2012; pp. 6–12.
10. De Cooman, B.C.; Chin, K.; Kim, J. High Mn TWIP steels for automotive applications. In *New Trends and Developments in Automotive System Engineering*; Chiaberge, M., Ed.; InTech: Rijeka, Croatia, 2010; pp. 101–128.
11. Bracke, L.; Verbeken, K.; Kestens, L.; Penning, J. Microstructure and texture evolution during cold rolling and annealing of a high Mn TWIP steel. *Acta Mater.* **2009**, *57*, 1512–1524. [CrossRef]
12. Steineder, K.; Schneider, R.; Krizan, D.; Bèal, C.; Sommitsch, C. Microstructural evolution of two low-carbon steels with a medium manganese content. In Proceedings of the 2nd HMnS Conference, Aachen, Germany, 31 August–4 September 2014; pp. 351–354.
13. De Cooman, B.C.; Speer, J. Quench and partitioning steel: A new AHSS concept for automotive anti-intrusion applications. *Steel Res. Int.* **2006**, *77*, 634–640. [CrossRef]

14. Steineder, K.; Krizan, D.; Schneider, R.; Bèal, C.; Sommitsch, C. On the microstructural characteristics influencing the yielding behavior of ultra-fine grained medium-Mn steels. *Acta Mater.* **2017**, *139*, 39–50. [CrossRef]
15. Speer, J.; Matlock, D.; De Cooman, B.C.; Schroth, J. Carbon partitioning into austenite after martensite transformation. *Acta Mater.* **2003**, *51*, 2611–2622. [CrossRef]
16. Speer, J.; Aussunção, F.; Matlock, D.; Edmonds, D. The "quenching and partitioning" process: Background and recent progress. *Mater. Res.* **2005**, *8*, 417–423. [CrossRef]
17. Edmonds, D.; He, K.; Rizzo, F.; De Cooman, B.C.; Matlock, D.; Speer, J. Quenching and partitioning martensite—A novel steel heat treatment. *Mater. Sci. Eng. A* **2006**, *438–440*, 25–34. [CrossRef]
18. Arlazarov, A.; Gouné, M.; Bouaziz, O.; Hazotte, A.; Petitgand, G.; Barges, P. Evolution of microstructure and mechanical properties of medium Mn steels during double annealing. *Mater. Sci. Eng. A* **2012**, *542*, 31–39. [CrossRef]
19. Huyghe, P.; Dépinoy, S.; Caruso, M.; Mercier, D.; Georges, C.; Malet, L.; Godet, S. On the effect of Q&P processing on the stretch-flange-formability of 0.2C Ultra-high Strength Steel Sheets. *ISIJ Int.* **2018**, *58*, 1341–1350.
20. Speer, J.; Streicher, A.; Matlock, D.; Rizzo, F. Quenching and partitioning: A fundamentally new process to create high strength TRIP sheet microstructures. In Proceedings of the Austenite Formation and Decomposition, Chicago, IL, USA, 9–12 November 2003; pp. 505–522.
21. Van Bohemen, S.; Santofimia, M.; Sietsma, J. Experimental evidence for bainite formation below M_S in Fe-0.66C. *Scr. Mater.* **2009**, *58*, 488–491. [CrossRef]
22. Somani, M.; Porter, D.; Karjalainen, L.; Misra, R. On various aspects of decomposition of austenite in a high-silicon steel during quenching and partitioning. *Metall. Mater. Trans. A* **2013**, *45*, 1247–1257. [CrossRef]
23. Kim, D.; Speer, J.; De Cooman, B.C. Isothermal transformation of a CMnSi steel below the M_S temperature. *Metall. Mater. Trans. A* **2011**, *42*, 1575–1585. [CrossRef]
24. Clarke, A.; Speer, J.; Miller, M.; Hackenberg, R.; Edmonds, D.; Matlock, D.; Rizzo, F.; Clarke, K.; De Moor, E. Carbon partitioning to austenite from martensite or bainite during the quench and partition (Q&P) process: A crictial assessment. *Acta Mater.* **2008**, *56*, 16–22.
25. Zakerinia, H.; Kermanpur, A.; Najafizadeh, A. Color metallography: A suitable method for characterization of martensite and bainite in multiphase steels. *Int. J. ISSI* **2009**, *6*, 14–18.
26. Wirthl, E.; Pichler, A.; Angerer, R.; Stiaszny, P.; Hauzenberger, K.; Titovets, Y.F.; Hackl, M. Determination of the volume amount of retained austenite and ferrite in small specimens by magnetic measurements. In Proceedings of the International Conference on TRIP-aided high strength ferrous alloys, Ghent, Belgium, 19–21 June 2002; pp. 61–64.
27. Koistinen, D.; Marburger, R. A general equation prescribing the extent of the austenite-martensite transformation in pure iron-carbon alloys and plain carbon steels. *Acta Metall.* **1959**, *7*, 59–60. [CrossRef]
28. Mahieu, J.; Maki, J.; De Cooman, B.C.; Claessens, S. Phase transformation and mechanical properties of Si-free CMnAl transformation-induced plasticity-aided steel. *Metall. Mater. Trans. A* **2002**, *33*, 2573–2580. [CrossRef]
29. Wang, G.; Chen, S.; Liu, C.; Wang, C.; Zhao, X.; Xu, W. Correlation of isothermal bainite transformation and austenite stability in quenching and partitioning steels. *J. Iron Steel Res. Int.* **2017**, *24*, 1095–1103.
30. Smanio, V.; Sourmail, T. Effect of partial martensite transformation on bainite reaction kinetics in different 1%C steels. *Solid State Phenom.* **2011**, *172–174*, 821–826. [CrossRef]
31. Bhadeshia, H.K.D.H.; Honeycombe, R. The bainite reaction. In *Steels—Microstructure and Properties*, 3rd ed.; Edward Arnold: London, UK, 2006; pp. 121–124.
32. Oka, M.; Okamoto, H. Swing back in kinetics near M_S in hypereutectoid steels. *Metall. Trans. A* **1988**, *19*, 447. [CrossRef]
33. Steineder, K.; Schneider, R.; Krizan, D.; Bèal, C.; Sommitsch, C. Investigation on the microstructural evolution in a medium-Mn steel (X10Mn5) after intercritical annealing. *HTM* **2015**, *70*, 19–25. [CrossRef]
34. De Moor, E.; Lacroix, S.; Clarke, A.; Penning, J.; Speer, J. Effect of retained austenite stabilized via quench and partitioning on the strain hardening of martensitic steels. *Metall. Mater. Trans. A* **2008**, *39*, 2586–2595. [CrossRef]
35. Grajcar, A.; Skrzypczyk, P.; Kozlowska, A. Effects of temperature and time of isothermal holding on retained austenite stability in medium-Mn steels. *Appl. Sci.* **2018**, *8*, 2156. [CrossRef]

36. Jimenez-Melero, E.; Van Dijk, N.; Zhao, L.; Sietsma, J.; Offerman, S.; Wright, J.; Van der Zwaag, S. Martensitic transformation of individual grains in low-alloyed TRIP steels. *Scr. Mater.* **2007**, *56*, 421–424. [CrossRef]
37. Kim, S.; Lee, J.; Barlat, F.; Lee, M.G. Transformation kinetics and density models of quenching and partitioning (Q&P) steels. *Acta Mater.* **2016**, *109*, 394–404.